A novel multiple change detection approach based on tri-temporal logic-verified change vector analysis in posterior probability space

Xin Wang [a], Peijun Du [b,*], Sicong Liu [c], Matthew Senyshen [d], Wei Zhang [b], Hong Fang [b], Xuanmei Fan [a,*]

[a] State Key Laboratory of Geohazard Prevention and Geoenvironment Protection, Chengdu University of Technology, Chengdu 610059, China
[b] School of Geography and Ocean Science, Nanjing University, Nanjing 210023, China
[c] College of Surveying and Geoinformatics, Tongji University, Shanghai 200092, China
[d] Department of Geography and Planning, Queen's University, Kingston K7L 3N6, Canada

ARTICLE INFO

ABSTRACT

Detailed land cover change trajectory offers a better opportunity for understanding the dynamic of land surface process. However, change information contained in training samples, which are usually difficult to obtain, needs to be provided in advance to achieve such goal within a complex scenario. A novel multiple change detection approach, namely Tri-temporal Logic-verified Change Vector Analysis (TLCVA) in posterior Probability Space (TLCVAPS), was proposed in this paper. It removes the dependence on change class information contained in training samples, while reducing the detection errors by taking change logic into account for the first time. The proposed approach consists of three steps, including: (1) change vector produced in posterior probability space, (2) binary change detection via TLCVA, and (3) change trajectory identification through combining change vector angle comparison and logic verification in change pattern. We applied the proposed approach on three tri-temporal datasets obtained in Nanjing, Xianning, and Zhenjiang, China, respectively. The results confirmed the superiority of TLCVAPS in comparison with state-of-the-art multiple change detection methods with the same prior knowledge.

1. Introduction

Land cover change, which offers valuable environmental information, is one of the most important indicators in geoscience related knowledge (Feddema et al. 2005). In recent years, with the increasing disturbances of anthropogenic activities, land cover has changed significantly (Zalles et al. 2021). Therefore, tracking change information is of great significance to ecological environment protection and sustainable development (Homer et al. 2015). Remote sensing enhances the traditional way of in-situ investigation, and provides effective means for obtaining repeated observations in wide geographic areas (Bruzzone and Bovolo 2013; Woodcock et al. 2020). An immense amount of multi-temporal data archives have been produced and utilized based on various satellites and sensor platforms. With the growth and accumulation of available remote sensing images, urgent demands of utilizing these data for detecting land cover changes are accordingly increasing (Roy et al. 2014; Wulder et al. 2019).

Change detection is a process to distinguish differences in images of the same scene acquired on different dates (Bovolo and Bruzzone 2007; Singh 1989). Up to the present, a great many of remote sensing-based change detection techniques have been successively proposed and applied in diverse fields, such as natural disaster interpretation, land degradation monitoring, and urbanization analysis (Wang et al. 2020a; Wang et al. 2022; Xian and Homer 2010). They can be broadly divided into unsupervised and supervised approaches. Unsupervised methods usually conduct a direct spectral comparison for different images. They do not require prior knowledge of a specific area, which is beneficial to capture the unexpected changes, such as flood, earthquake, landslide, etc. (Falco et al. 2013; Hostache et al. 2012; Wang et al. 2022). Nevertheless, unsupervised change detection outcomes are susceptible to external contributors, such as atmospheric condition changes, illumination differences, insufficient sensor calibration, etc., which usually occur between multi-temporal images at different acquisition dates (Chen et al. 2005; Solano-Correa et al. 2018). By contrast, the requirements of the supervised methods in radiometric consistency are not as strict as those of unsupervised methods. The model trained by a

supervised classifier is highly adaptable, which greatly reduces the impacts of the variance in image acquisition conditions (Tan et al. 2019). Furthermore, tracking change trajectory can also be realized through a supervised method with the help of training samples. According to the aforementioned advantages, supervised methods have been successfully applied in many change detection applications (Volpi et al. 2013; Wang et al. 2020b; Wu et al. 2017).

The overwhelming majority of supervised change detection tasks are based on bi-temporal or time series images. For bi-temporal change detection, pre- and post-classification are the two widely adopted strategies (Peiman 2011). Post classification comparison (PCC) obtains result from two classified images acquired at different time (Coppin et al. 2004). As long as land cover properties of some pixels are obtained in advance, the change locations with their trajectories can be achieved accordingly. However, misclassification in any image will lead to a biased result because of error propagation (Burnicki et al. 2010). In contrast, pre-classification methods, which identify changes via classifying stack or difference image, do not rely on land cover information of any temporal images (Volpi et al. 2013). This kind of approaches consider the feature variance between different images and require the samples contained change class information once. Nevertheless, the change information contained in training samples is difficult to obtain. For time series change detection, it is possible to extract change information by PCC image-by-image or classifying the stacked images for a fixed time period. However, with the accumulative effect in time series images, the aforementioned defects in bi-temporal change detection are greatly magnified (Kempeneers et al. 2012). Model-based methods, which take the long-term change patterns of pixel values into account, open up a new path for time series change detection (Verbesselt et al. 2010; Zhu 2017). As typical a representative, Continuous Change Detection and Classification construct a harmonic function based on land surface reflectance of each pixel in a given time series (Zhu and Woodcock 2014). They are capable of achieving not only land cover type but also change trajectory at any time. Deep learning-based methods are also effective time series change detection techniques, which enable to fully mine the high-level spectral, spatial, and temporal characteristics of time series data through a pre-trained model, realizing the purpose of precisely monitoring continuous land cover changes (Kong et al. 2018; van Duynhoven and Dragićević 2019). However, whether it is a harmonic model or deep network model, they both require large amounts of dense data to fit complicated functions or train sophisticated models, consuming more time and labor in data acquisition and program computing even with the purpose of detecting changes over several instant times.

Since bi-temporal and time series change detection cannot meet the requirements of high accuracy and efficiency simultaneously, the pattern of land surface change among several images is therefore discovered and extracted as auxiliary knowledge to make full use of temporal information. Circular change detection approach derived from 2D phase unwrapping provides the ability to identify the errors between images pairs within the time sequence (Bertoluzza et al. 2017). Its accuracy improves with the increase of images considered in an iteration. Consequently, a better performance comes with more computing power, running time, and obtained images. Tri-temporal Logic-verified Change Vector Analysis (TLCVA), which analyzes the logical relationship among three images acquired from different dates, was proposed by Du et al. (2020). It overcomes the shortcomings of bi-temporal change detection through additional time information, and avoids the onerous work of iterative test or time series model construction. However, without prior knowledge, TLCVA is powerless to identify detailed change category. According to the current research, two crucial issues should be further addressed:

(1) How to reduce the dependence on change class information contained in training samples while avoiding error accumulation in multiple change detection problems?

(2) How to take the advantage of temporal characteristic between several images to make up for the deficiency of change class identification with spectral features?

Therefore, Tri-temporal Logic-verified Change Vector Analysis in posterior Probability Space (TLCVAPS) is proposed in this paper, which is developed upon the TLCVA. In this approach, the magnitude of change vector is utilized to identify the unchanged and changed regions, whereas the direction of change vector is adopted to track the change trajectories. Furthermore, a change pattern system is constructed by the change detection results of three bi-temporal image pairs, whose consistency in change pattern are examined, to ensure their logical rationality in temporal space. Three case studies using tri-temporal SPOT 7, Sentinel-2, and Landsat 8 remote sensing datasets were carried out, confirming the effectiveness and superiority of TLCVAPS.

2. Method

The proposed change detection method mainly includes the following parts: (1) change vector produced in posterior probability space, (2) binary change detection based on TLCVA, and (3) change trajectory identification and logical verification. Fig. 1 displays the flowchart of the TLCVAPS.

2.1. Change vector produced in posterior probability space

CVA is a basic change detection method, which obtained changes by comparing pixel-based reflectance (Lambin and Strahlers 1994; ZhiYong et al. 2021). Based on this theory, CVAPS is developed by pixel-wise posterior probability comparison instead, reducing the impacts affected by radiometric variation between different images (Chen et al. 2011). Posterior probability provides the ability to denote the reliability of identification result (Tao et al. 2005). It can be estimated by a function of image features in a supervised classifier:

$$P = f(x) \tag{1}$$

where $x = (x_1, x_2, ..., x_m)$ represents image features of a pixel. m denotes the feature dimension. $P = (p_1, p_2, ..., p_n)$ represents the posterior probabilities of the pixel attached to land cover class 1 to n, in which n is the class number. Let class probabilities of a pixel in time 1 and 2 be $P^1 = (p_1^1, p_2^1, ..., p_n^1)^T$ and $P^2 = (p_1^2, p_2^2, ..., p_n^2)^T$, the change vector in CVAPS can be described as follows:

$$\overrightarrow{\Delta P} = P^2 - P^1 = \begin{Bmatrix} p_1^2 - p_1^1 \\ p_2^2 - p_2^1 \\ \cdots \cdots \\ p_n^2 - p_n^1 \end{Bmatrix} \tag{2}$$

where $\overrightarrow{\Delta P}$ is change vector and can model change characteristics. The magnitude of the corresponding change vector can be represented by.

$$|\overrightarrow{\Delta P}| = \sqrt{\left(p_1^2 - p_1^1\right)^2 + \left(p_2^2 - p_2^1\right)^2 + ... + \left(p_n^2 - p_n^1\right)^2} \tag{3}$$

Then, a threshold for change magnitude can be determined to examine if a pixel has changed. Furthermore, change trajectory can be defined according to the direction of change vector $\overrightarrow{\Delta P}$. We use $P = (p_1, p_2, ..., p_n)$ to denote the posterior probabilities of a pure pixel belonging to class e:

$$p_{ei} = \begin{cases} 1, & \text{if } i = e \\ 0, & \text{if } i \neq e \end{cases} \tag{4}$$

where $e, i \in [1, n]$. Assuming that a pure pixel changes from land cover type a to b, the base change vector is defined as follows:
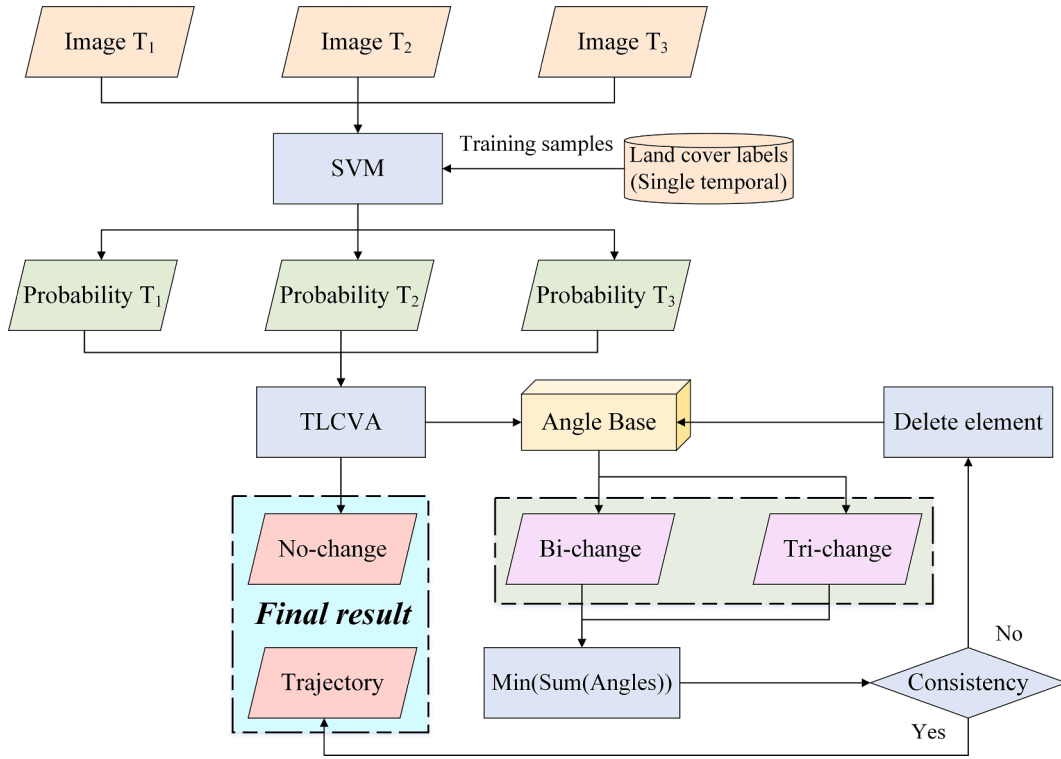
Fig. 1. Flowchart of the TLCVAPS method.

$$\overrightarrow{\Delta P}_{ab} = P_b^2 - P_a^1 \tag{5}$$

where $P_a^1 = (p_{a1}^1, p_{a2}^1, ..., p_{an}^1)^T$ and $P_b^2 = (p_{b1}^2, p_{b2}^2, ..., p_{bn}^2)^T$. The angle between $\overrightarrow{\Delta P}$ and base change vector $\overrightarrow{\Delta P}_{ab}$ can be considered as a measure of their similarity. Thus, a group of base change vector $\left\{ \overrightarrow{\Delta P}_{ab} \middle| a, b = 1, 2, ..., n \text{ and } a \neq b \right\}$ can be used to identify the trajectory of change vector $\overrightarrow{\Delta P}$. Given that $\overrightarrow{\Delta P}_{kl} \in \left\{ \overrightarrow{\Delta P}_{ab} \right\}$ has the smallest angle with $\overrightarrow{\Delta P}$, indicating the most similar change pattern between $\overrightarrow{\Delta P}_{kl}$ with $\overrightarrow{\Delta P}$, the change trajectory of $\overrightarrow{\Delta P}$ is identified as from land cover type k to l. $\overrightarrow{\Delta P}_{kl}$ can be calculated through the following formula:

$$\overrightarrow{\Delta P}_{kl} = \underset{a,b}{\mathrm{argmin}} \left\{ \arccos \frac{\overrightarrow{\Delta P} \cdot \overrightarrow{\Delta P}_{ab}}{|\overrightarrow{\Delta P}||\overrightarrow{\Delta P}_{ab}|} \right\} \tag{6}$$
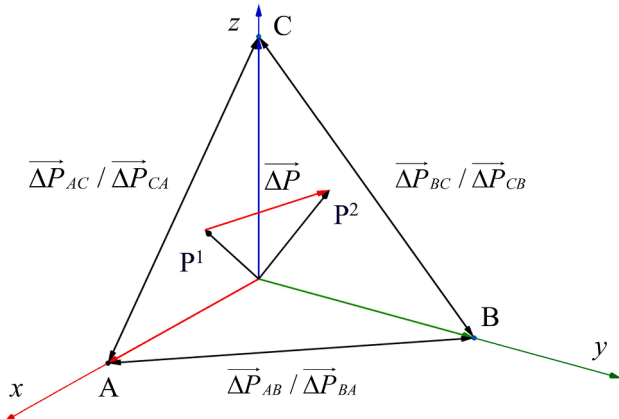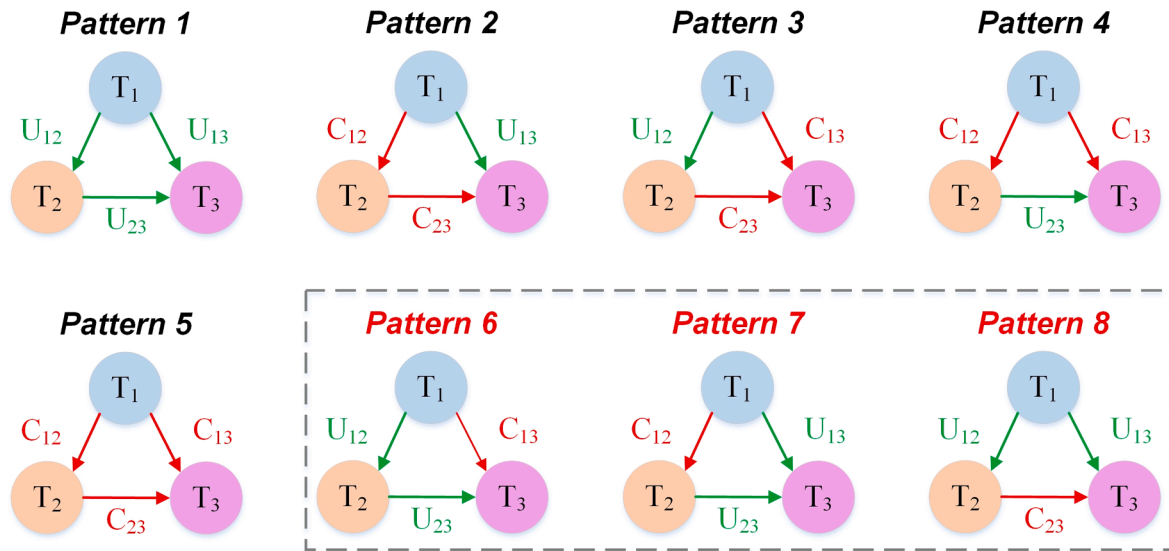

Fig. 2. Sketch map of posterior probability-based change vector.

The geometric interpretation is displayed in Fig. 2, in which the axes represent the posterior probabilities of three land cover types. Three vertices A, B, and C on the axes denote pure pixels belong to three definite classes, and thus the borders of the black triangle denote three base change vectors. P^1 and P^2 denote pixel posterior probabilities of a pixel in time 1 and 2, and thus $\overrightarrow{\Delta P}$ represents the corresponding change vector. Since the angle between $\overrightarrow{\Delta P}$ and $\overrightarrow{\Delta P}_{AB}$ of the base change vectors is the smallest, the change trajectory of $\overrightarrow{\Delta P}$ is defined as land cover type A to B. Note that when P^1 and P^2 are exactly the same, $\overrightarrow{\Delta P}$ is consequently $\overrightarrow{0}$, which means that the reflection of these pixels are completely consistent and can be directly considered as no-change.

2.2. Binary change detection based on TLCVA

For the case of tri-temporal images, change detection can be conducted by separating them into three pairs of bi-temporal images. A change path is then constructed in acquisition order. From the perspective of mathematics, each pixel has two possible outcomes (change or no-change) from an image pair, and one of 2^3 types of change patterns can be generated. However, in reality the sequence of land cover changes over a path must keep consistent, which means that three of 2^3 aforementioned patterns do not conform the realistic logic due to false and missed detection in bi-temporal change detection outcome. Fig. 3 displays the change patterns of tri-temporal change detection, in which Pattern 6 to 8 are illogical.

Therefore, TLCVA approach is adopted to correct the mistakes in bi-temporal change detection, which mainly contains the three parts (Du et al. 2020). First, basic CVA, in which change vectors are generated in posterior probability space, is implemented and the incorrect patterns are identified through logic judgement. Then, automated sample decision (ASD), which is based on the judgement whether a bi-temporal result affects the reasonability of the correct change pattern, is utilized to obtain training samples. The reliable samples are selected based on the following rules: Given three bi-temporal results are within a correct

Fig. 3. Change patterns of tri-temporal change detection. Note that U_{rs} and C_{rs} denote unchanged and changed pixels between a bi-temporal image pair T_r and T_s, respectively.

change pattern, if changing a certain one results in unreasonable logic, it is considered as a reliable sample label. In contrast, it does not affect the reasonability of the logic, it can be seen as an unreliable sample and will not be used in the subsequent processing. The defined training samples are then used for updating the outcomes within the incorrect patterns. Finally, reliability comparison is carried out to address the remaining illogical patterns. It is worth noting that the change vector in the original TLCVA characterizes the image differences by spectral reflectance, whose direction is not suitable for identifying the type of land cover changes. Instead, the posterior probability of land cover, whose difference is more conducive to depicting the trajectory information for changes as is shown in Fig. 2, is adopted here.

2.3. Change trajectory identification and logic verification

After implementing TLCVA, change and no-change in a tri-temporal pattern can be defined. As change vectors between each image pair are achieved, the trajectories of changed pixels can be calculated by comparing the angles between the change vectors and the base change vectors. According to the theory of unsupervised TLCVA presented in 2.2, there are three cases for the five logical tri-temporal change patterns: a change pattern contains zero, two or three changes. For a pixel position, if there are p change vectors between an image pair, p^q possible change trajectory combinations can be acquired (q is the number of changes contained in a tri-temporal change pattern).

We assume that each bi-temporal image pair contains three possible change types: 1) For the case with three changes in a pattern (Fig. 3 - Pattern 5), 3^3 possible change trajectories can be concluded theoretically. How to locate the exact one is the key issue. Similar to the criterion of finding the minimum angle between the change vector and the base change vector in bi-temporal change detection, the way of identifying the correct tri-temporal change trajectory is to find the one with the minimum sum of three bi-temporal change vector angles. Therefore, the sum of the angles for each change trajectory at a pixel location is therefore calculated in advance, constructing a three-dimensional sum change vector angle cube (SCVAC). By locating the position of the minimum element in SCVAC, the change trajectory of the pixel in tri-temporal images can be finally achieved.

$$S = \min \sum_{h=1}^{u} \theta_h \qquad (7)$$

where θ_h represents the minimum angle between the change vector

and base change vectors of the hth pair of bi-temporal images. u is the number of changes in a change pattern. S indicates the minimum sum of bi-temporal change vector angles in the change pattern. 2) For the case with two changes in a pattern (Fig. 3 - Pattern 2 to 4), the unchanged border is directly output as no-change, and the other two changed borders can produce 3^2 possible change trajectories. The sum angles at a pixel location are then calculated, constructing a two-dimensional sum change vector angle plane (SCVAP). Similarly, by searching the element with a minimum value, change trajectories of the pixel location among tri-temporal images can be consequently achieved. 3) For the case with no change in a pattern (Fig. 3 - Pattern 1), they are directly output as no-changes. Fig. 4 illustrates the steps of achieving the change trajectories of a pixel in the case of three changes in a change pattern.

As a tri-temporal change trajectory is obtained by locating the minimum element, their logic in tri-temporal change path requires quality control. The beginning and the end of the change path from T_{12} to T_{23} must be consistent with T_{13}. (Note that the change vector of an unchanged pixel is defined as $\vec{0}$.) If they are inconsistent, the corresponding element will be abandoned from SCVAC or SCVAP. The minimum value will be then reselected from the remaining elements until the consistency condition of the two paths are satisfied. Accordingly, the corresponding change trajectory of tri-temporal images is determined.

To better express its entire implementation, the detailed steps of the proposed change detection approach are summarized in the following pseudocode.

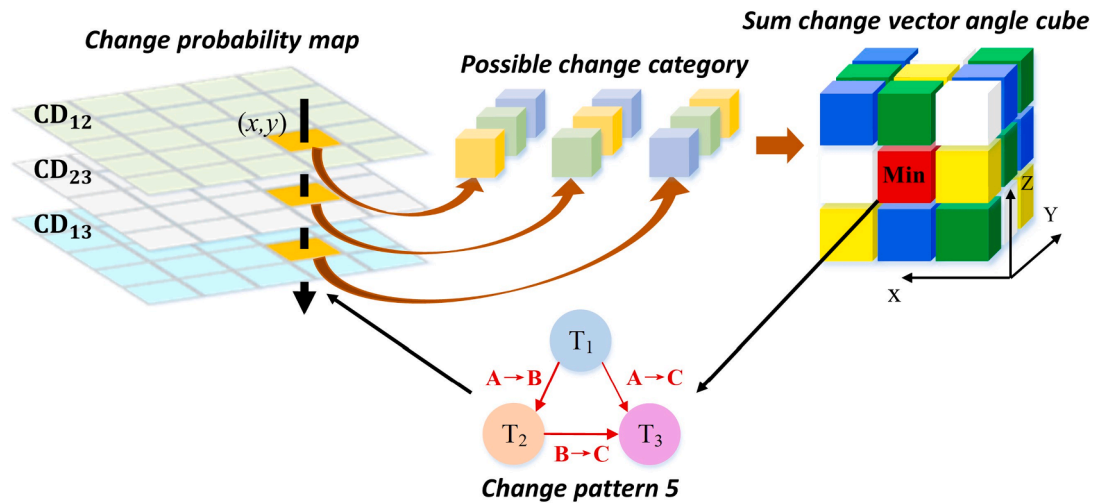| **TLCVAPS Algorithm** |
| --- |
| **Input**: land cover map D of a single temporal image |
| Step 1: Unsupervised TLCVA is conducted in advance to determine the pixel positions belong to change pattern 1 |
| Step 2: Training samples randomly chosen at these positions from land cover map D |
| Step 3: A general classifier model for tri-temporal images is trained via the single temporal training samples, |
| and a posterior probability is produced for each pixel in tri-temporal images |
| Step 4: Differences of posterior probability are used as change vectors to identify the change areas via TLCVA |
| Step 5: SCVAC or SCVAP is constructed at each pixel location by summing the angles between change vectors and |
| base change vectors of three bi-temporal image pairs |
| **For** Go through each pixel location |
| Step 6: Search the index with minimum value in SCVAC or SCVAP |
| **While** The consistency of two change path in a change pattern is not satisfied |
| Step 7: Eliminate the minimum value in SCVAC or SCVAP of the pixel |

Fig. 4. Illustration of identifying change trajectories by TLCVAPS in the case of three changes in a tri-temporal change pattern.

(continued)

TLCVAPS Algorithm
Step 8: Continue searching the index with minimum value in SCVAC or SCVAP
End while
Step 8: Identify change trajectory between each bi-temporal image pair at the pixel location
End For
Output: Final multiple change trajectory results Y through tri-temporal images

3. Results and analysis

3.1. Dataset description

A. Dataset I: Nanjing (Simulated SPOT 7 images).

This dataset was simulated on a tri-temporal SPOT 7 image with four multispectral bands acquired over an area of Nanjing, China. The original image was obtained on March 27, 2017. A subset of the image was selected as the first temporal image T_1 with a size of 171×332 pixels. It contains four land cover types including vegetation, bare land, impervious surface area (ISA) and water. To construct a multiple change
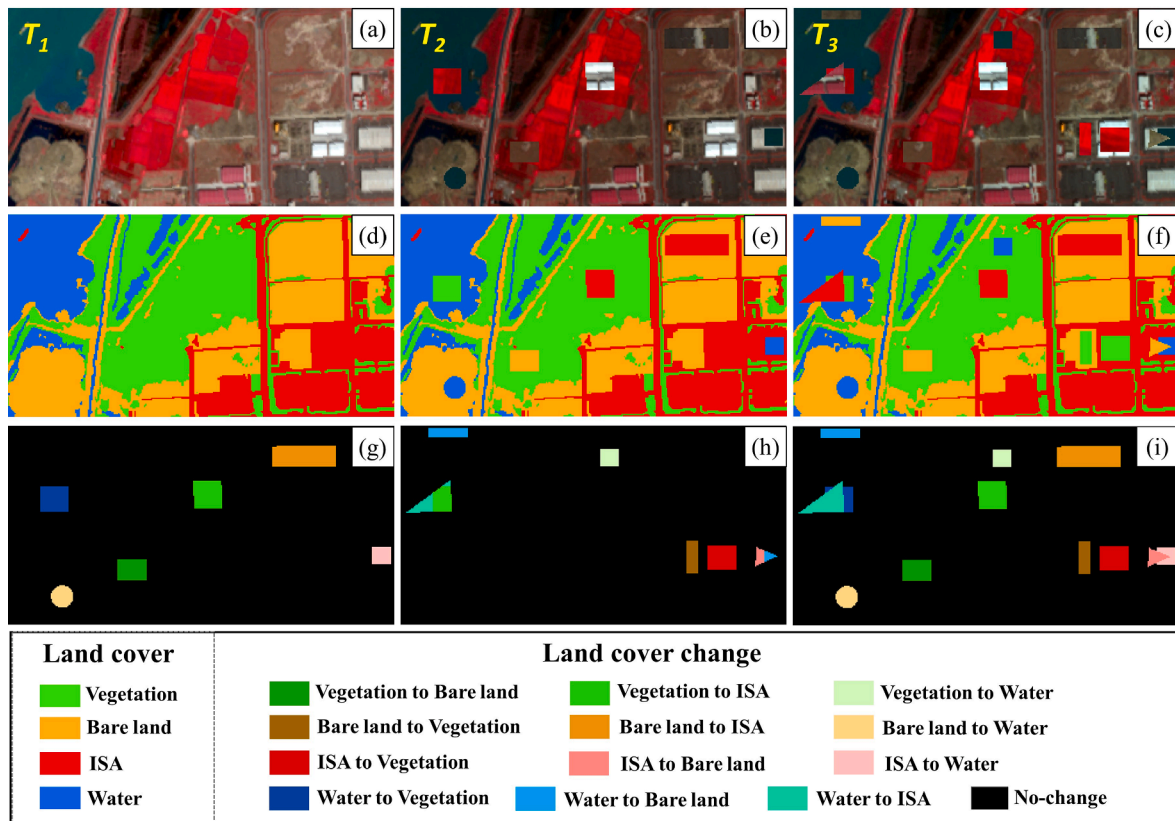

Fig. 5. SPOT 7 Nanjing dataset. (a)-(c) are the tri-temporal images. (d)-(f) are the land cover maps of T_1 to T_3. (g)-(i) are the reference maps of CD_{12}, CD_{23}, and CD_{13}, respectively.

detection problem, some pixels in image T_1 assigned to different land cover classes were moved to a different location with all bands, simulating a new image as T_2. Taking image T_2 as the benchmark, image T_3 was constructed in the same way. In addition, small different values were added into the pixels of T_2 and T_3 (DN = +10 and −50 for T_2 and T_3, respectively) to simulate constant bias in atmospheric or illumination conditions. We also appended white gaussian noise into T_2 and T_3 with different signal-to-noise ratio (SNR) values (20 and 30 dB for T_2 and T_3, respectively) to enhance the complexity of the task. These steps help to generate a tri-temporal simulated remote sensing dataset with images T_1, T_2, and T_3. False color composites of the dataset are displayed in Fig. 5 (a)-(c). Land cover types of pre- and post-change in tri-temporal images are also displayed in Fig. 5 (d)-(f) for T_1 to T_3, respectively. Accordingly, the corresponding change reference maps are achieved and presented in Fig. 5 (g)-(i) through the calculation of pixel movement, which contains a category of unchanged pixels and 12 categories of changed pixels in CD_{12} (change detection between T_1 and T_2), CD_{23} (change detection between T_2 and T_3) and CD_{13} (change detection between T_1 and T_3). Table.1 lists the detailed land cover changes and the corresponding pixel amounts in the reference maps.

B. Dataset II: Xianning (Real Sentinel-2 images).

This dataset consists of tri-temporal Sentinel-2 images acquired on 2016–12-09, 2017–12-09, and 2017–12-24 in Xianning, China, which were obtained from Copernicus Data Hub. The reflectance image of Level L1C were transformed to Level L2A. Ten bands, including Band 2–8, 8A, 11–12, were selected and resampled to 10 m for each image of the dataset. Image-to-image radiometric correction and co-registration (residual error within 0.5 pixel) were conducted to reduce discrepancies and accurately match the pixels in the same location. Subsets of the images with a size of 273×251 pixels were defined as T_1, T_2, and T_3, which contain four land cover types including vegetation, bare land, sand and water. In this scenario, the land cover changed significantly during these periods, such as the vegetation change by cultivation, the coastal change under the tidal forces, et.al. The tri-temporal images with false color composite are shown in Fig. 6 (a)-(c). With prior knowledge and Google Earth historical images, careful manual image interpretation for land cover type and change was conducted. The reference land cover maps of T_1 to T_3 are shown in Fig. 6 (d)-(f), and the corresponding reference change maps are displayed in Fig. 6 (g)-(i), in which one class of no-change and four classes of change are included. The detailed pixel amounts of land cover changes in the reference maps are listed in Table 2.

C. Dataset III: Zhenjiang (Regional Landsat 8 images).

The land covers and their transitions will be complex in a large area, leading to more types of land cover changes naturally formed. Therefore, to prove the effectiveness of the proposed approach, we applied it on a wide-area application. The third dataset covers a region of Zhenjiang, China, with an area of more than 174 km^2. The dataset consists of tri-temporal Landsat 8 OLI images with 7 bands (Band 2–7 and 10) with a resolution of 30 m. Pre-processing including relative radiometric

correction and image co-registration (residual error within 0.5 pixel) were implemented to ensure the consistencies of reflection and location among multi-temporal images. Three images were acquired on 2017–05-18, 2019–05-24, and 2021–03-26, during which this area underwent a rapid urbanization and the farming status of agricultural land were also significantly different. The images in false color composite are displayed in Fig. 7 (a)-(c). For the reference maps, we adopted the following strategies to achieve. We first manually labeled four land cover samples, and utilized multiple machine learning-based (Support Vector Machine, Random Forest, Rotation Forest, Extreme Learning Machine) and deep learning-based (Convolutional Neural Network) models to perform training and classification for each image. The pixels with the same classification results of all the classifiers are retained, and the remaining are visually interpreted by cooperating with the Geographic National Condition Census (GNCC) and higher resolution images (multi-temporal Sentinel-2 data and Google Earth historical images). The reference land cover maps (Fig. 7 (d)-(f)) and their corresponding change transition maps (Fig. 7 (g)-(i)) were finally obtained at 30 m resolution level. It is worth noting that our interpretation of each image represents the land cover at the corresponding moment. For example, under the impact of crop phenology, the land cover of a pixel, where the rice is farmed in the period of water storage, ear, and harvesting, will be recognized as water, vegetation, and bare land, respectively. Meanwhile, the types of land cover changes can be greatly enriched under this circumstance. Table.3 lists the detailed land cover changes and the corresponding pixel amounts in the reference maps.
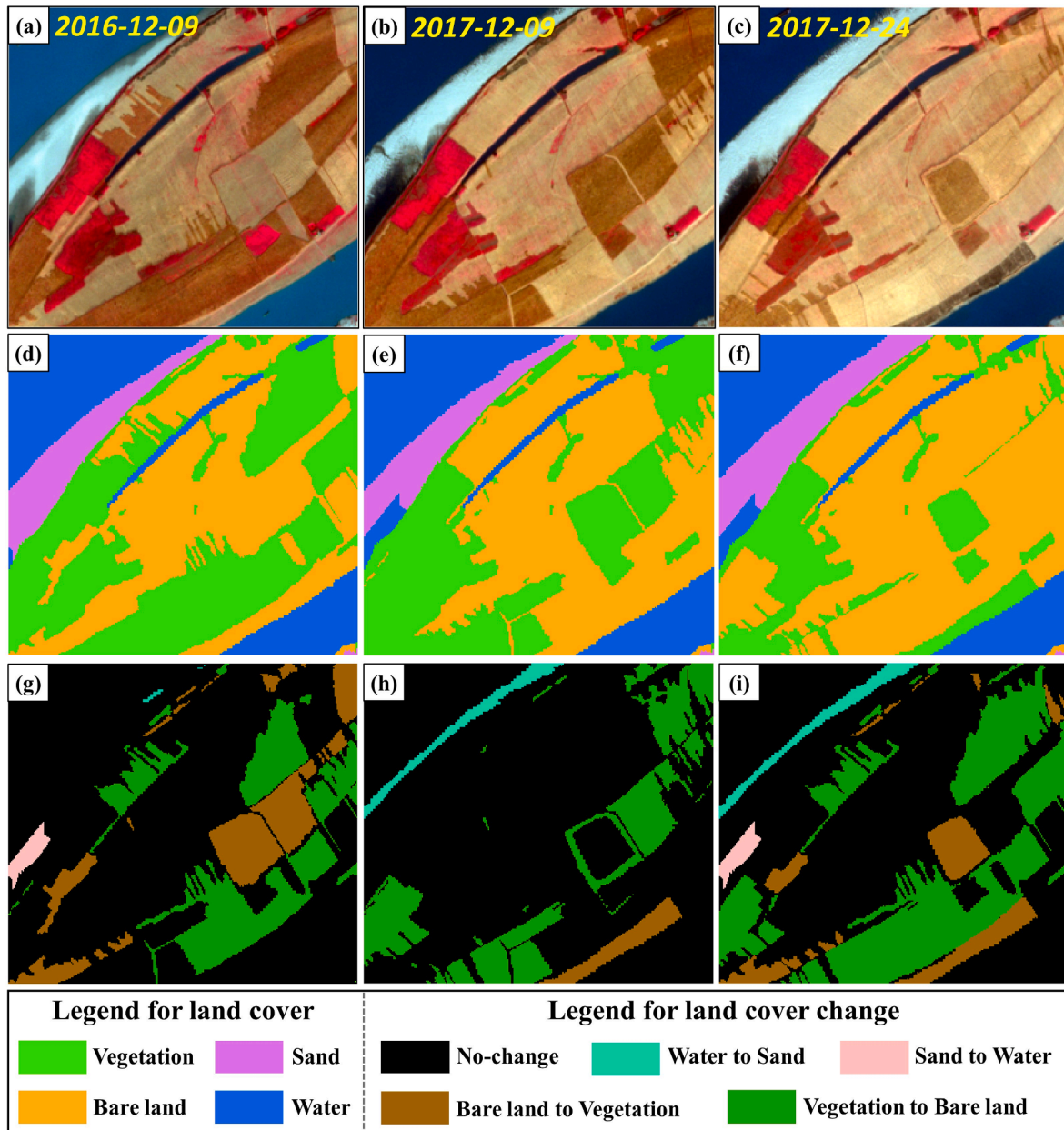
3.2. Experimental setting

To confirm the superiority of TLCVAPS, three multiple change detection methods were carried out. The first one was PCC, which identified change trajectory though the classification results obtained at different dates (Serra et al. 2003). In PCC experiments, training samples were randomly chosen from the land cover of temporal 1 to train a classifier model, which was then employed to tri-temporal image T_1 to T_3 to obtain the respective land cover classification results. Consequently, land cover change can be achieved through the comparison of classification results at different dates. The second one was derived from Chen et al. (2012) (ULCM hereafter). We modified its framework to be suitable for tri-temporal method, which contained three crucial steps: 1) Training samples were randomly selected from the land cover of T_1 to train the classifier model and applied it to T_1 to T_3, achieving the classification results C_1, C_2, and C_3 and the posterior probability vectors of T_{12} and T_{13}. 2) Changed and unchanged areas in T_2 and T_3 were then detected by conducting CVAPS on T_{12} and T_{13}. 3) The land cover types of changed pixels in T_2 and T_3 were updated from classification results C_2 and C_3, whereas the unchanged pixels inherited the land cover from C_1. The last comparative method was derived from Saha et al. (2019) (DCVA hereafter). We made appropriate adjustments to the method to enable comparative analysis under the same experimental conditions: 1) Deep features were extracted and selected by Convolutional Neural Network with the architecture we proposed in Fang et al. (2022), which is proved to be more effective for change detection with training samples provided, instead of the pre-trained network, through the training samples randomly chosen from the land cover of T_1. 2) Deep feature-based classifications were conducted to obtain the land cover C_1, C_2, and C_3, while deep feature-based CVA were carried out to achieve the changed and unchanged region in CD_{12} and CD_{13}. 3) The land cover types of changed pixels in T_2 and T_3 were updated by C_2 and C_3, whereas the land cover types of unchanged pixels were inherited from C_1.

In terms of parameter settings, SVM was selected to generate the classification results and their posterior probability in the aforementioned methods (except for DCVA) owing to its robustness in dealing with ill-posed issues. Although deep learning-based techniques are proved to be effective, their complicated network structures usually leading to lower efficiencies. Besides, their performances are not as good

Table 1
Pixel amounts of reference land cover change maps in the Nanjing dataset.

Category	CD_{12}	CD_{23}	CD_{13}
No-change	53,695	54,769	52,072
Vegetation to Bare land	450	/	450
Vegetation to ISA	585	323	585
Vegetation to Water	/	240	240
Bare land to Vegetation	/	280	280
Bare land to ISA	986	/	986
Bare land to Water	288	/	288
ISA to Vegetation	/	525	525
ISA to Bare land	/	96	153
ISA to Water	240	/	183
Water to Vegetation	528	/	205
Water to Bare land	/	329	272
Water to ISA	/	210	533

Fig. 6. Sentinel-2 Xianning dataset. (a)-(c) are the tri-temporal images in chronological order. (d)-(f) are the land cover maps of T_1 to T_3. (g)-(i) are the reference maps of CD_{12}, CD_{23}, and CD_{13}, respectively.

Table 2

Pixel amounts of reference land cover change maps in Xianning dataset.

Transition category	CD_{12}	CD_{23}	CD_{13}
No-change	50,355	55,322	44,518
Vegetation to Bare land	10,666	10,398	17,381
Bare land to Vegetation	6854	1465	4638
Sand to Water	594	/	594
Water to Sand	54	1338	1392

as expected when dealing with insufficient training samples. In contrast, SVM provides the advantages of parameter insensitivity and strong generalization, which are beneficial to address the problems with a small sample size or a non-linear model (Maulik and Chakraborty 2017). The Gaussian kernel was adopted for SVM, whose parameters were chosen through Particle Swarm Optimization, an adaptive optimization method for searching the optimum parameters (Del Valle et al. 2008).

The sizes of image patches used for model training in the SPOT 7, Sentinel-2, and Landsat 8 datasets were set as 7×7, 5×5, and 3×3 pixels in DCVA method, respectively. The Otsu algorithm, which is an effective non-parametric method for image segmentation, was adopted for threshold decision of change magnitude in ULCM, DCVA, and TLCVAPS (Otsu 1979). The outcomes of these approaches were obtained through the mean of 10 Monte Carlo runs to avoid the random errors in the experiments.

3.3. Change detection

A. SPOT 7 Nanjing Dataset.

In the experiment of Nanjing dataset, we assumed that the one with prior knowledge is image T_1. 40 labels in each land cover type of T_1 were randomly chosen as training samples to train SVM, which was applied to produce the posterior probability and change vector in TLCVAPS. Under the same parameter condition, PCC, ULCM, and DCVA were also carried
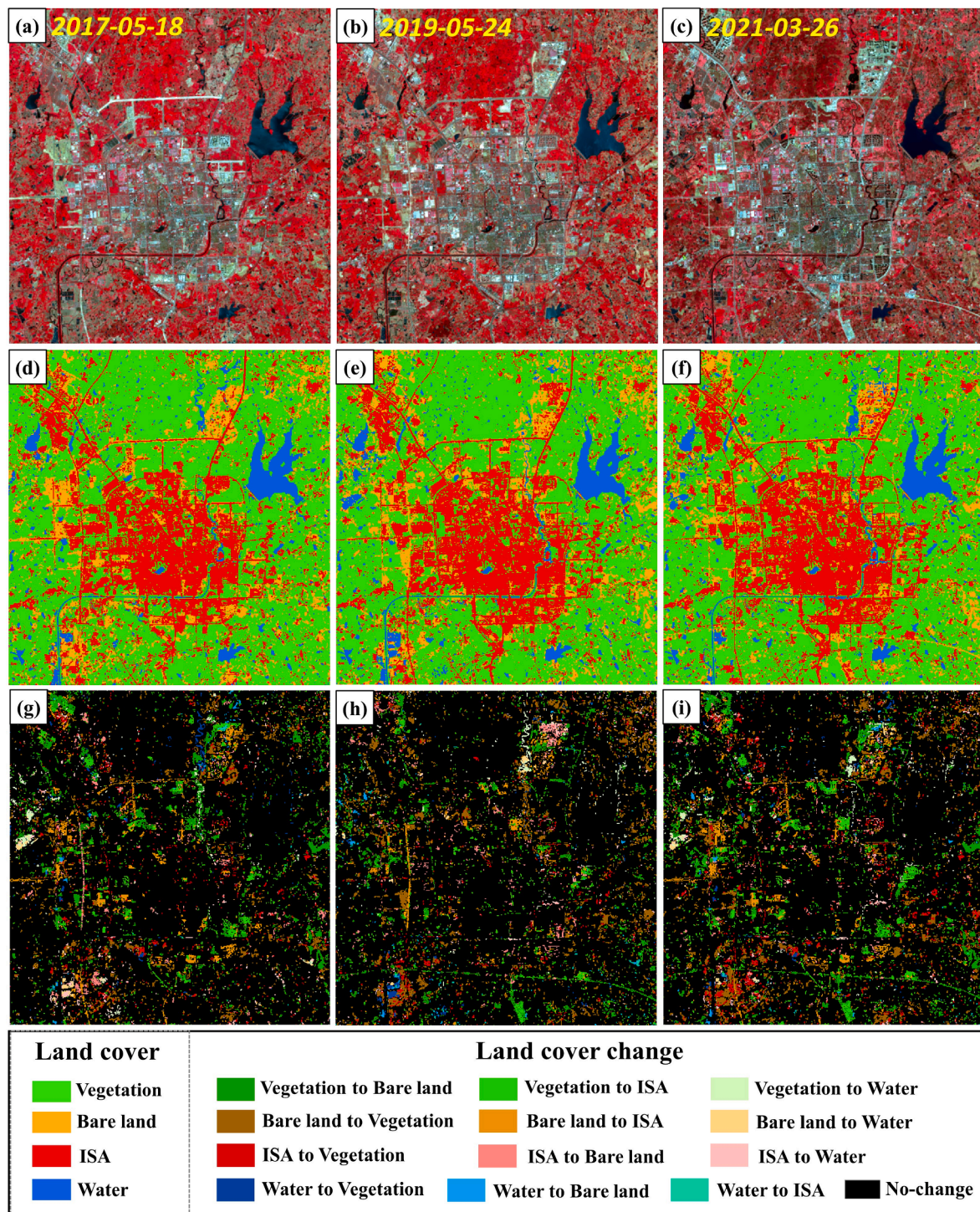
Fig. 7. Landsat 8 Zhenjiang dataset. (a)-(c) are the tri-temporal images in chronological order. (d)-(f) are the land cover maps of T_1 to T_3. (g)-(i) are the reference maps of CD_{12}, CD_{23}, and CD_{13}, respectively.

out. Comprehensive evaluations were conducted in terms of change detection maps and accuracy indices. Table.4 lists the assessment of the methods for Nanjing dataset, where the best indices were emphasized in bold. It can be concluded that the results of TLCVAPS outperformed the other three methods. From the aspect of overall accuracy, TLCVAPS achieved the best overall accuracies with 99.82%, 99.31% and 99.17% in CD_{12}, CD_{23} and CD_{13}, respectively. Their corresponding Kappa coefficients were also the highest among all the methods, proving its effectiveness and reliability. From the perspective of binary (change/no-change) result, TLCVAPS achieved the lowest commission and omission

errors and the highest F1 scores in most bi-temporal image pairs. More specifically, PCC was on par with TLCVAPS in the aspect of independent accuracy of change class, but its accuracies of unchanged class were far behind, resulting in a comprehensive performance inferior to TLCVAPS. ULCM was not as eye-catching as the other methods in terms of independent accuracy, but its overall accuracy and reliability were better than PCC in CD_{12} and CD_{13}. Especially in CD_{12}, its performance was close to that of TLCVAPS. The accuracies of DCVA for no-change were close to those of TLCVAPS, but the accuracies of independent change class were worse, resulting in inferior overall performances to TLCVAPS

Table 3
Pixel amounts of reference land cover change maps in the Zhenjiang dataset.

Category	CD_{12}	CD_{23}	CD_{13}
No-change	162,455	163,461	156,337
Vegetation to Bare land	9155	6435	8732
Vegetation to ISA	3141	3486	5579
Vegetation to Water	949	852	1246
Bare land to Vegetation	6519	10,416	9971
Bare land to ISA	3730	2129	3375
Bare land to Water	450	291	352
ISA to Vegetation	2846	2020	4153
ISA to Bare land	2224	2351	1881
ISA to Water	855	597	816
Water to Vegetation	710	618	544
Water to Bare land	252	319	286
Water to ISA	214	525	228

but better than PCC and ULCM.

Fig. 8 displays the change detection maps produced by different methods applied to Nanjing dataset. The following results can be noticed. PCC detected changes by comparing their classification results, and many obvious continuous false detections at the edge of the ground object occurred in the change detection maps, leading to much lower no-change accuracies and higher commission errors. More than that, the constant bias and white Gaussian noise had a significant impact on the classification results, giving a great influence on the results. However, this kind of errors can be eliminated by analyzing the change vectors. Judging from the maps produced by ULCM, the identification of changed area in CD_{12} was accurate, whereas more missed detections occurred in CD_{13} and CD_{23}, indicating that the land cover posterior probability of image T_3 was not as accurate as that of image T_2 through the classifier model trained by T_1. The change trajectory detected based on CVAPS may be affected by different image acquisition conditions, resulting in missed or false detection. Compared to PCC and ULCM, DCVA and TLCVAPS both avoided most missed and false detections caused by classification confusion and additional noise. TLCVAPS was better at detecting the edges of changed objects than DCVA through the analysis of change vector magnitude and direction with logic verification in temporal space.

B. Sentinel-2 Xianning Dataset.

Similarly, to access the quantitative evaluation of the change detection approaches, a detailed assessment was conducted for the Xianning dataset. We also assumed that the one with prior knowledge is image T_1. Then, 35 labeled samples in each class were chosen at random as training samples to train the SVM model for generating posterior probability and change vector in TLCVAPS. PCC, ULCM, and DCVA were carried out with the same parameters. Table.5 lists the accuracy assessment of the aforementioned methods, where the best results were highlighted in bold. Regardless of the change detection accuracy of any bi-temporal image pairs, TLCVAPS consistently obtained the best performance compared to the other methods. In detail, TLCVAPS achieved the highest overall accuracies of 90.78%, 90.25%, and 87.64% with Kappa coefficients of 0.7864, 0.7181, and 0.7532 in CD_{12}, CD_{23}, and CD_{13}, respectively. Meanwhile, TLCVAPS obtained the lowest commission and omission errors (except for CD_{12}) and the highest F1 scores (except for CD_{13}) in terms of binary change detection indices. For the accuracy of individual change class, TLCVAPS was capable of achieving the highest accuracies in most cases.

The change detection maps created with different methods for Xianning dataset are displayed in Fig. 9. The yellow dashed circles exemplify the improvements of TLCVAPS compared to the other methods. PCC obtained more commission errors, owing to the combined effect of misclassification and error propagation. For instance, obvious false detections of the change class 'water to vegetation' occurred along the southeast riparian zone in CD_{12} and CD_{13}, because the mixtures of water and vegetation were provided with similar surface reflectance values for the water class. Thus, the water body was mistakenly classified as vegetation in the second and third temporal images, resulting in these false detections. Similar errors also occurred in the center of CD_{23} and the central south of CD_{13}. In addition to false detection, missed detections existed as well, such as in the southwest area of CD_{13}. For the results of ULCM, errors were significantly less than PCC, since it avoided the process of error accumulation by analying the posterior probability-based change vectors, improving the performance to a certain extent. In contrast, DCVA greatly reduced salt-and-pepper noise due to the consideration of scene-based deep features. However, false and missed detections of an entire object sometimes occurred (e.g., false detection of water to vegetation in the west of CD_{23} and CD_{13}). The change detection maps of TLCVAPS indicated significant improvements compared to the other methods. It not only utilized temporal information to address the problem of false and missed detections, but also adopted the direction of the change vector instead of the classification comparison to avoid change class confusion caused by error propagation.

Table 4
Change detection results achieved by different methods in the Nanjing dataset.

Index	CD_{12}				CD_{23}				CD_{13}			
	PCC	ULCM	DCVA	TLCVAPS	PCC	ULCM	DCVA	TLCVAPS	PCC	ULCM	DCVA	TLCVAPS
NC (%)	86.23	99.80	99.60	**99.91**	89.19	87.52	99.35	**99.86**	76.90	86.90	99.40	**99.78**
V-B (%)	**99.78**	98.44	82.22	99.56	/	/	/	/	98.67	96.89	78.00	**98.89**
V-I (%)	**100.00**	90.94	97.78	**100.00**	**100.00**	99.69	**100.00**	99.69	**100.00**	96.41	96.75	**100.00**
V-W (%)	/	/	/	/	**100.00**	98.75	66.25	**100.00**	**100.00**	98.75	66.25	**100.00**
B-V (%)	/	/	/	/	45.36	72.14	**97.86**	47.14	68.57	72.14	**97.86**	47.14
B-I (%)	97.87	95.84	2.84	**97.97**	/	/	/	/	**98.48**	98.28	0.51	98.07
B-W (%)	99.65	98.96	66.67	**100.00**	/	/	/	/	**100.00**	98.96	60.07	**100.00**
I-V (%)	/	/	/	/	**100.00**	96.76	75.24	**100.00**	**100.00**	96.76	75.24	**100.00**
I-B (%)	/	/	/	/	100.00	100.00	81.25	100.00	99.35	98.04	88.24	96.08
I-W (%)	**99.58**	73.33	49.58	87.08	/	/	/	/	96.72	81.97	22.95	89.07
W-V (%)	100.00	100.00	99.05	100.00	/	/	/	/	100.00	100.00	81.95	100.00
W-B (%)	/	/	/	/	**58.97**	42.86	14.29	51.98	**50.74**	37.50	5.88	44.49
W-I (%)	/	/	/	/	93.33	**97.62**	90.48	96.19	99.06	98.87	98.12	98.31
OA (%)	86.93	99.51	97.38	**99.82**	89.04	87.45	98.43	**99.31**	78.36	87.35	96.12	**99.17**
Kappa	0.4225	0.9529	0.7024	**0.9829**	0.3529	0.3206	0.7683	**0.9023**	0.3805	0.5227	0.7143	**0.9475**
p	<0.01	<0.01	<0.01	<0.01	<0.01	<0.01	<0.01	<0.01	<0.01	<0.01	<0.01	<0.01
CE (%)	13.77	0.20	0.40	**0.09**	10.81	12.48	0.65	**0.14**	23.10	13.10	0.60	**0.22**
OE (%)	**0.05**	0.29	2.26	0.09	0.03	0.05	0.80	**0.01**	0.06	0.21	3.18	**0.09**
F1	0.4524	0.9801	0.9343	**0.9915**	0.4020	0.3670	0.8952	**0.9815**	0.4372	0.5742	0.9363	**0.9873**

Note that the abbreviations in the table are as follows. NC: No-change. V-B: vegetation to bare land. V-I: vegetation to ISA. V-W: vegetation to water. B-V: bare land to vegetation. B-I: bare land to ISA. B-W: bare land to water. I-V: ISA to vegetation. I-B: ISA to bare land. I-W: ISA to water. W-V: water to vegetation. W-B: water to bare land. W-I: water to ISA. OA: overall accuracy. p: p value for significant test. CE: commission error. OE: omission error. F1: F1 score.
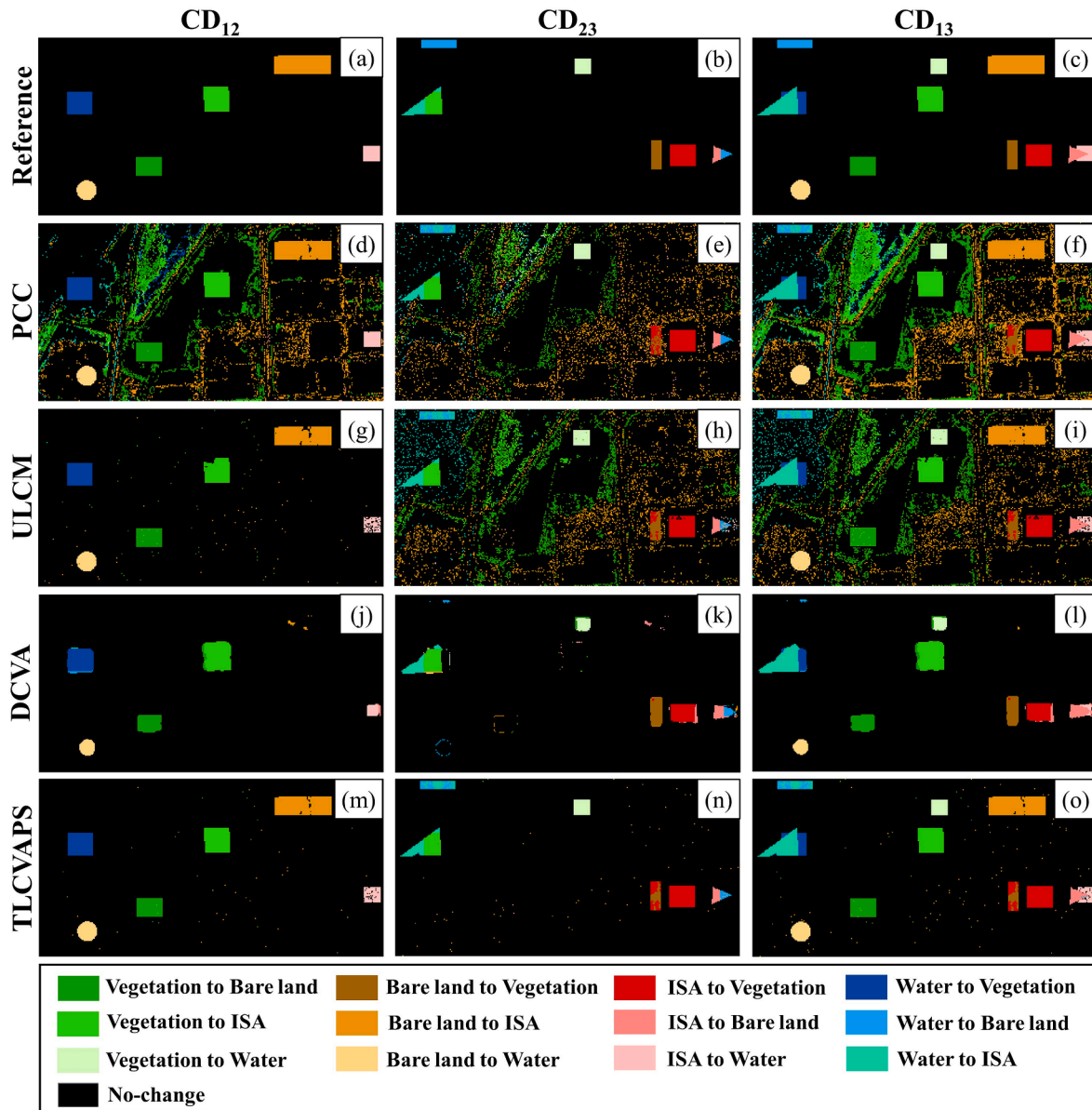
Fig. 8. Tri-temporal change detection results of the Nanjing dataset. (a)-(c), (d)-(f), (g)-(i), (j)-(l), and (m)-(o) are the reference maps, PCC, ULCM, DCVA, and TLCVAPS results for CD_{12}, CD_{23}, and CD_{13}, respectively.

Table 5
Change detection results achieved by different methods in the Xianning dataset.

Index	CD_{12}				CD_{23}				CD_{13}			
	PCC	ULCM	DCVA	TLCVAPS	PCC	ULCM	DCVA	TLCVAPS	PCC	ULCM	DCVA	TLCVAPS
NC (%)	89.61	93.39	**96.28**	93.39	89.29	90.07	**92.89**	92.75	89.67	92.21	**96.47**	92.39
V-B (%)	90.62	89.65	74.34	90.51	81.55	79.41	65.77	**85.31**	93.03	91.42	73.41	90.94
B-V (%)	**79.06**	70.09	56.38	76.16	**57.54**	46.08	59.11	49.62	28.44	24.49	**74.28**	37.45
S-W (%)	37.04	35.19	46.13	**49.66**	/	/	/	/	36.36	34.34	**23.40**	49.66
W-S (%)	**64.81**	53.70	38.89	22.22	50.52	62.93	53.44	**69.43**	70.19	69.32	**59.12**	78.09
OA (%)	88.24	89.94	**88.39**	90.78	86.68	86.98	87.28	**90.25**	85.52	86.46	**87.73**	87.64
Kappa	0.7399	0.7639	**0.7027**	0.7864	0.6253	0.6265	0.6076	**0.7181**	0.7124	0.7236	0.7456	**0.7532**
p	<0.01	<0.01	<0.01	<0.01	<0.01	<0.01	<0.01	<0.01	<0.01	<0.01	<0.01	<0.01
CE (%)	10.39	6.61	**3.72**	6.61	10.71	9.93	**7.11**	7.25	10.33	7.79	**3.53**	7.61
OE (%)	**5.52**	6.81	11.14	5.82	5.38	5.89	7.94	**3.68**	10.69	11.76	12.64	**9.53**
F1	0.8350	0.8700	0.8771	**0.8772**	0.7614	0.7670	0.7889	**0.8351**	0.8479	0.8619	**0.8957**	0.8781

C. Landsat 8 Zhenjiang Dataset.

We also implemented a quantitative evaluation for this regional case. In the experiment, T_1 was assigned as the one with prior knowledge, and

35 labeled samples of each class for this image were randomly selected as the training samples for model learning in all the methods. Table 6 lists their performances in multiple aspects. Similarly, it can be observed
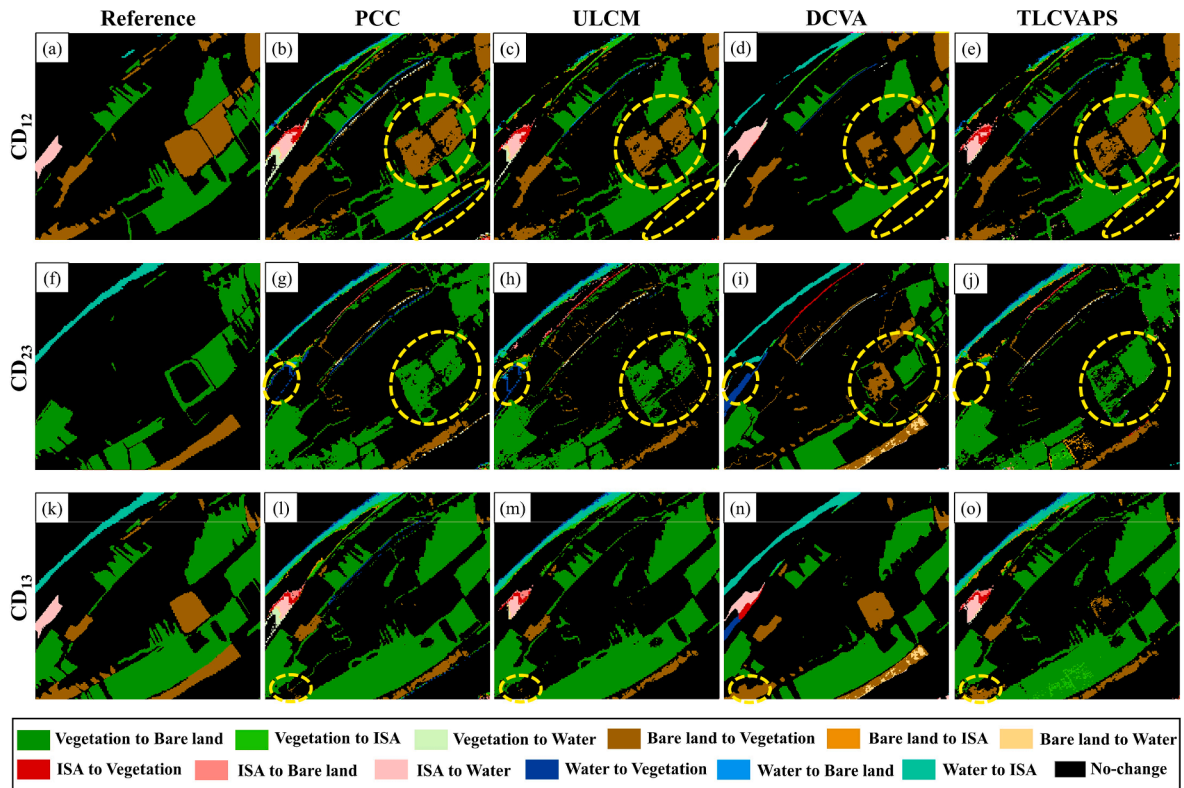
Fig. 9. Tri-temporal change detection results of the Xianning dataset. The first to the last row are the CD_{12}, CD_{23}, and CD_{13} results for Reference, PCC, ULCM, DCVA, and TLCVA, respectively.

that the TLCVAPS outperformed the other listed methods in terms of overall accuracy and Kappa coefficients for CD_{12}, CD_{23}, and CD_{13}. In more detail, it also achieved highest accuracy for each independent change class. From the perspective of binary change detection performance, TLCVAPS obtained the lowest omission errors in all conditions and the highest or the second highest F1 scores in most cases. DCVA did well in detecting unchanged region with the best performances in no-change class accuracy and commission error in each case. In contrast, PCC and ULCM underperformed the DCVA and TLCVAPS by any measure. The change trajectory maps of the listed methods for the Zhenjiang dataset are displayed in Fig. 10.
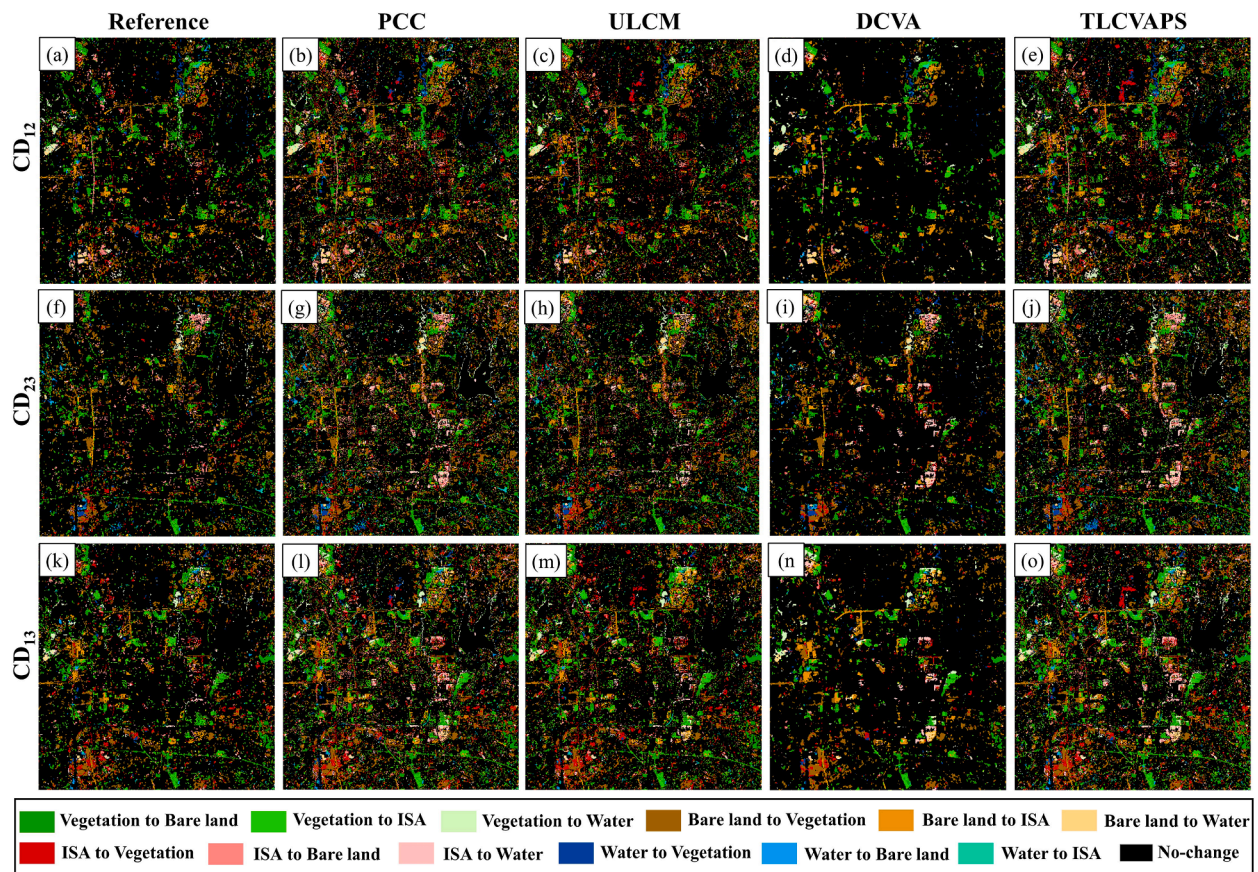
4. Discussion

4.1. Training sample analysis

The supervised change detection is susceptible to the amount of training samples. Sufficient training samples enables to make the model trained more adaptable, whereas excessive training samples increase the cost of manual labeling and reduce the efficiency of model training. Therefore, it is of great significance to select the appropriate amount of training samples according to different research areas. To investigate its specific impact on the results of TLCVAPS, increasing amounts of training samples chosen from the land cover map corresponding to a

Table 6
Change detection results achieved by different methods in the Zhenjiang dataset.

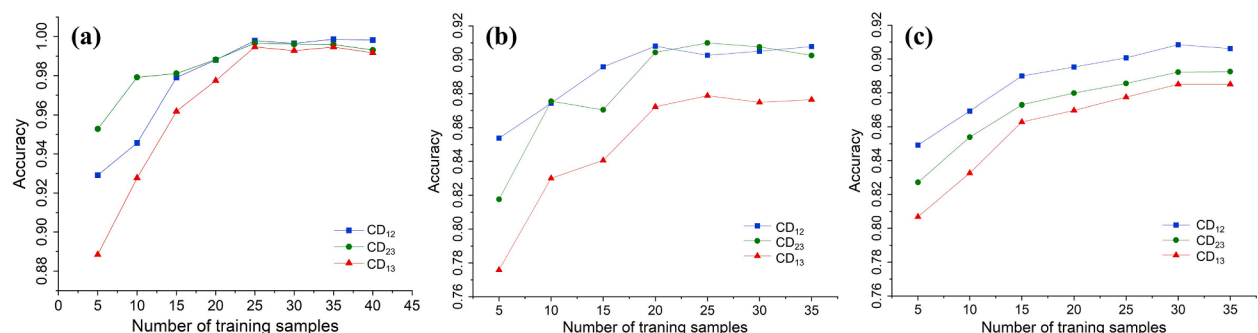| Index	CD_{12}				CD_{23}				CD_{13}			
	PCC	ULCM	DCVA	TLCVAPS	PCC	ULCM	DCVA	TLCVAPS	PCC	ULCM	DCVA	TLCVAPS
NC (%)	88.12	92.07	**96.48**	90.35	87.17	88.88	**92.81**	89.35	86.26	90.53	**94.58**	88.00
V-B (%)	89.00	80.39	40.99	**94.10**	86.87	76.60	33.57	**95.32**	86.44	73.61	36.89	**94.19**
V-I (%)	86.02	86.72	48.20	**92.84**	81.01	80.03	23.52	**88.93**	83.22	83.33	38.45	**90.86**
V-W (%)	77.34	63.33	45.63	**84.72**	81.34	60.09	30.75	**92.61**	82.34	64.93	43.02	**94.86**
B-V (%)	86.30	80.00	37.61	**95.11**	85.01	73.99	40.00	**86.28**	86.48	77.92	51.67	**91.42**
B-I (%)	83.24	76.92	51.74	**87.72**	80.23	73.60	42.79	**86.57**	77.99	73.10	49.81	**80.27**
B-W (%)	81.11	60.44	66.22	**91.33**	83.51	52.23	50.86	**96.56**	76.99	55.11	50.85	**93.18**
I-V (%)	81.41	79.66	11.42	**89.63**	72.08	72.43	17.82	**84.36**	82.88	81.19	22.97	**90.54**
I-B (%)	83.18	68.39	26.84	**85.88**	75.97	51.60	19.06	**80.94**	81.55	61.83	13.34	**81.92**
I-W (%)	87.72	71.11	14.74	**90.99**	82.75	67.67	23.95	**96.31**	91.42	74.88	13.24	**96.45**
W-V (%)	79.58	62.96	31.55	**93.80**	74.11	52.27	43.85	**84.63**	74.82	49.45	34.01	**87.50**
W-B (%)	70.63	32.94	35.32	**93.25**	73.35	23.20	18.81	**95.30**	73.08	19.23	22.03	**95.80**
W-I (%)	80.37	64.49	24.30	**92.52**	86.10	66.67	8.76	**93.33**	85.09	63.16	7.89	**87.72**
OA (%)	87.69	89.76	87.10	**90.61**	86.45	86.19	83.47	**89.25**	85.86	87.53	83.91	**88.50**
Kappa	0.6570	0.6854	0.4734	**0.7320**	0.6183	0.5894	0.3676	**0.6908**	0.6569	0.6697	0.4653	**0.7192**
p	<0.001	<0.001	<0.001	<0.001	<0.001	<0.001	<0.001	<0.001	<0.001	<0.001	<0.001	<0.001
CE (%)	11.88	7.93	**3.52**	9.65	12.83	11.12	**7.19**	10.65	13.74	9.47	**5.42**	12.00
OE (%)	2.16	3.02	9.59	**1.08**	2.60	3.60	9.88	**1.32**	2.78	3.94	11.10	**1.26**
F1	0.7369	0.7938	**0.7992**	0.7863	0.7077	0.7205	0.6697	**0.7595**	0.7481	**0.7958**	0.7759	0.7866

Fig. 10. Tri-temporal change detection results of the Zhenjiang dataset. The first to the last row are the CD$_{12}$, CD$_{23}$, and CD$_{13}$ results for Reference, PCC, ULCM, DCVA, and TLCVA, respectively.

single temporal image were tested. Fig. 11 shows the overall accuracies in these circumstances. They reveal a noticeable increase when the numbers in each class are <25 (Nanjing dataset), 20 (Xianning dataset), and 30 (Zhenjiang dataset), whereas they tend to stabilize afterwards. Thus, the results demonstrate that an appropriate quantity of training samples are capable of obtaining the outcomes with satisfactory accuracy.
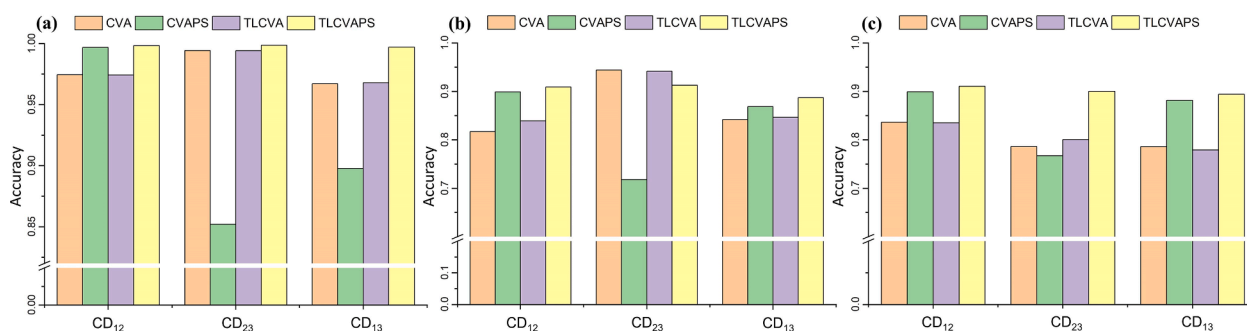
4.2. Binary change analysis

In addition to using the direction of change vector instead of post classification comparison to make an improvement, TLCVAPS is novel at using land surface change patterns to further examine the self-consistency of tri-temporal change trajectory. To prove the importance of temporal information, the binary change detection results of the datasets with (TLCVAPS) and without (CVA, CVAPS) logic verification

were generated by controlling variables. Their overall accuracies are presented in Fig. 12. It can be noticed from the figure that the accuracies of TLCVAPS are higher than those of CVAPS and CVA for each image pair regardless of the datasets, indicating the vital contribution of temporal logic. From another perspective, in comparison to CVA and TLCVA, TLCVAPS employs posterior probability difference instead of radiometric difference to detect changes, avoiding the strict requirement of radiometric correction. Therefore, TLCVAPS provides the ability of monitoring land cover change with large areas and long time. Fig. 12 also demonstrates this advantage by comparing TLCVAPS with CVA and TLCVA. Besides, the change magnitudes of different transition categories in posterior probability space are normalized in the same scale of 0 to 1. Hence, it is more appropriate to use a single threshold, which is easier to be optimized, for TLCVAPS than TLCVA and CVA.

Fig. 11. Overall accuracies of the (a) Nanjing dataset, (b) Xianning dataset, and (c) Zhenjiang dataset through TLCVAPS with different quantities of training samples.

Fig. 12. Comparison of binary change detection performance of CVA, CVAPS, TLCVA, and TLCVAPS in the (a) Nanjing dataset, (b) Xianning dataset, and (c) Zhenjiang dataset.

4.3. Time consumption analysis

To assess the efficiency of the TLCVAPS, computational time of the adopted methods in all the datasets were recorded and listed in Table 7. The experiments were conducted using MATLAB R2021a on Intel (R) Core (TM) i9-11900 K PC machine with 3.50 GHz of CPU and 64 GB of RAM. With additional combination of loop computation of minimum sum of change vector angle and logical verification for each change pattern, the time consumption of TLCVAPS is more than three times that of PCC and ULCM. However, it took less time than DCVA, in which the structure of deep neural network is complicated, and parameter optimization and model training are time-consuming. From a comprehensive perspective, it is worthwhile and feasible to sacrifice a little efficiency for more accurate and reliable change detection results.

5. Conclusion

A novel multiple change detection approach, TLCVAPS, is proposed in this paper. Its main contributions are concluded as following: First, TLCVAPS improves the performance of multiple change detection by using land cover information of single temporal image, which gets rid of the dependence on change class information contained in training samples, significantly reducing the difficulty and cost of sample acquisition compared to state-of-the-art supervised multiple change detection methods. Again, TLCVAPS adopts the angle between the change vectors as the basis to recognize the land cover transition, successfully avoiding the error accumulation by comparing classification results at different dates. Lastly, TLCVAPS is the first attempt to introduce temporal logic into multiple change detection task with several instant images provided, which is a pilot research for the utilization of time information. Experiments of three tri-temporal remote sensing datasets were carried out, and their results confirmed the superiority of TLCVAPS in terms of accuracy and reliability. Given its effectiveness and accuracy, the proposed multiple change detection approach enables to help policy makers and practitioners better understand the process of land surface development, and has great potential be applied in urban land use planning, environmental governance, natural hazard assessment, etc.

Although both TLCVAPS and TLCVA are the change detection methods based on tri-temporal remote sensing images, they have obvious differences, including the following aspects. (1) Target difference: TLCVA is a binary change detection method, in which the results are change and no-change. While TLCVAPS is designed for multiple change detection, whose results not only indicate whether a pixel has changed or not, but also include the transition trajectory between different land cover classes for the changed pixels. (2) Method differences: TLCVA adopts the magnitude of change vector to characterize intensity of land cover change at different dates and identify whether a pixel change or not. Then, it utilizes the logical relationship in tri-temporal image change patterns to correct errors. In contrast, TLCVAPS not only adopts the magnitude of change vector to recognize

Table 7
Time consumptions of different multiple change detection algorithms.

Case study	PCC	ULCM	DCVA	TLCVAPS
Nanjing	6.55 s	6.93 s	41.70 s	26.65 s
Xianning	7.78 s	8.12 s	51.29 s	39.13 s
Zhenjiang	20.66 s	25.16 s	96.83 s	85.50 s

whether a pixel change or not, but also uses the direction of change vector to analyze the trajectory of the changed pixel. In logic verification-based post-processing, compared to reclassification and posterior probability comparison for false and missed detection in TLCVA, the strategy of constantly screening the minimum sum of change vector angles until a logical self-consistency in each change pattern is implemented in TLCVAPS. Combining the above two aspects, TLCVAPS is a further extension and deepening of TLCVA in terms of target and method.

For the case of increasing or decreasing land cover types in a tri-temporal dataset, a possible solution is to label samples for the image with the most land cover types to train a general multi-class classifier, which is suitable for all images within the dataset. Consequently, the steps of the proposed approach can be executed as above and the corresponding results can be successfully achieved. Besides, since CVA-based methods recognize changes through the comparison of the instant status of land surface at different moments, seasonal changes in TLCVAPS will influence the land cover identification and its posterior probability value for an object, which will consequently affect the change vector between different times, leading to differences on change detection results. Hence, similar to other CVA-based methods, it is better to keep the phenological periods of multi-temporal images consistent when applying TLCVAPS approach.

CRediT authorship contribution statement

Xin Wang: Conceptualization, Methodology, Formal analysis, Writing – original draft. **Peijun Du:** Resources, Writing – review & editing, Project administration. **Sicong Liu:** Resources, Methodology. **Matthew Senyshen:** Methodology, Writing – review & editing. **Wei Zhang:** Data curation, Visualization. **Hong Fang:** Methodology, Validation. **Xuanmei Fan:** Writing – review & editing.

Declaration of Competing Interest

The authors declare that they have no known competing financial interests or personal relationships that could have appeared to influence the work reported in this paper.

References

Bertoluzza, M., Bruzzone, L., Bovolo, F., 2017. Circular change detection in image time series inspired by two-dimensional phase unwrapping. In: 2017 9th International Workshop on the Analysis of Multitemporal Remote Sensing Images (MultiTemp) (pp. 1-4): IEEE.

Bovolo, F., Bruzzone, L., 2007. A theoretical framework for unsupervised change detection based on change vector analysis in the polar domain. IEEE Trans. Geosci. Remote Sens. 45 (1), 218–236.

Bruzzone, L., Bovolo, F., 2013. A novel framework for the design of change-detection systems for very-high-resolution remote sensing images. Proc. IEEE 101 (3), 609–630.

Burnicki, A.C., Brown, D.G., Goovaerts, P., 2010. Propagating error in land-cover-change analyses: impact of temporal dependence under increased thematic complexity. International Journal of Geographical Information Science 24 (7), 1043–1060.

Chen, J., Chen, X., Cui, X., Chen, J., 2011. Change vector analysis in posterior probability space: A new method for land cover change detection. IEEE Geosci. Remote Sens. Lett. 8 (2), 317–321.

Chen, X., Chen, J., Shi, Y., Yamaguchi, Y., 2012. An automated approach for updating land cover maps based on integrated change detection and classification methods. ISPRS J. Photogramm. Remote Sens. 71, 86–95.

Chen, X., Vierling, L., Deering, D., 2005. A simple and effective radiometric correction method to improve landscape change detection across sensors and across time. Remote Sens. Environ. 98 (1), 63–79.

Coppin, P., Jonckheere, I., Nackaerts, K., Muys, B., Lambin, E., 2004. Review ArticleDigital change detection methods in ecosystem monitoring: a review. Int. J. Remote Sens. 25 (9), 1565–1596.

del Valle, Y., Venayagamoorthy, G.K., Mohagheghi, S., Hernandez, J.-C., Harley, R.G., 2008. Particle swarm optimization: basic concepts, variants and applications in power systems. IEEE Trans. Evol. Comput. 12 (2), 171–195.

Du, P., Wang, X., Chen, D., Liu, S., Lin, C., Meng, Y., 2020. An improved change detection approach using tri-temporal logic-verified change vector analysis. ISPRS J. Photogramm. Remote Sens. 161, 278–293.

Falco, N., Mura, M.D., Bovolo, F., Benediktsson, J.A., Bruzzone, L., 2013. Change detection in VHR images based on morphological attribute profiles. IEEE Geosci. Remote Sens. Lett. 10 (3), 636–640.

Fang, H., Du, P., Wang, X., 2022. A novel unsupervised binary change detection method for VHR optical remote sensing imagery over urban areas. Int. J. Appl. Earth Obs. Geoinf. 108, 102749. https://doi.org/10.1016/j.jag.2022.102749.

Feddema, J.J., Oleson, K.W., Bonan, G.B., Mearns, L.O., Buja, L.E., Meehl, G.A., Washington, W.M., 2005. The importance of land-cover change in simulating future climates. Science 310 (5754), 1674–1678.

Homer, C., Dewitz, J., Yang, L., Jin, S., Danielson, P., Xian, G., Coulston, J., Herold, N., Wickham, J., Megown, K., 2015. Completion of the 2011 National Land Cover Database for the conterminous United States–representing a decade of land cover change information. Photogramm. Eng. Remote Sens. 81, 345–354.

Hostache, R., Matgen, P., Wagner, W., 2012. Change detection approaches for flood extent mapping: How to select the most adequate reference image from online archives? Int. J. Appl. Earth Obs. Geoinf. 19, 205–213.

Kempeneers, P., Sedano, F., Strobl, P., McInerney, D.O., San-Miguel-Ayanz, J., 2012. Increasing robustness of postclassification change detection using time series of land cover maps. IEEE Trans. Geosci. Remote Sens. 50 (9), 3327–3339.

Kong, Y.-L., Huang, Q., Wang, C., Chen, J., Chen, J., He, D., 2018. Long short-term memory neural networks for online disturbance detection in satellite image time series. Remote Sensing 10 (3), 452. https://doi.org/10.3390/rs10030452.

Lambin, E.F., Strahlers, A.H., 1994. Change-vector analysis in multitemporal space: A tool to detect and categorize land-cover change processes using high temporal-resolution satellite data. Remote Sens. Environ. 48 (2), 231–244.

Maulik, U., Chakraborty, D., 2017. Remote Sensing Image Classification: A survey of support-vector-machine-based advanced techniques. IEEE Geosci. Remote Sens. Mag. 5 (1), 33–52.

Otsu, N., 1979. A threshold selection method from gray-level histograms. IEEE transactions on systems, man, and cybernetics 9 (1), 62–66.

Peiman, R., 2011. Pre-classification and post-classification change-detection techniques to monitor land-cover and land-use change using multi-temporal Landsat imagery: a case study on Pisa Province in Italy. Int. J. Remote Sens. 32 (15), 4365–4381.

Roy, D.P., Wulder, M.A., Loveland, T.R., C.e., W., Allen, R.G., Anderson, M.C., Helder, D., Irons, J.R., Johnson, D.M., Kennedy, R., Scambos, T.A., Schaaf, C.B., Schott, J.R., Sheng, Y., Vermote, E.F., Belward, A.S., Bindschadler, R., Cohen, W.B., Gao, F., Hipple, J.D., Hostert, P., Huntington, J., Justice, C.O., Kilic, A., Kovalskyy, V., Lee, Z. P., Lymburner, L., Masek, J.G., McCorkel, J., Shuai, Y., Trezza, R., Vogelmann, J., Wynne, R.H., Zhu, Z., 2014. Landsat-8: Science and product vision for terrestrial global change research. Remote Sens. Environ. 145, 154–172.

Saha, S., Bovolo, F., Bruzzone, L., 2019. Unsupervised deep change vector analysis for multiple-change detection in VHR images. IEEE Trans. Geosci. Remote Sens. 57 (6), 3677–3693.

Serra, P., Pons, X., Saurí, D., 2003. Post-classification change detection with data from different sensors: some accuracy considerations. Int. J. Remote Sens. 24 (16), 3311–3340.

Singh, ASHBINDU, 1989. Review article digital change detection techniques using remotely-sensed data. Int. J. Remote Sens. 10 (6), 989–1003.

Solano-Correa, Y., Bovolo, F., Bruzzone, L., 2018. An approach for unsupervised change detection in multitemporal VHR images acquired by different multispectral sensors. Remote Sensing 10 (4), 533. https://doi.org/10.3390/rs10040533.

Tan, K., Zhang, Y., Wang, X., Chen, Y.u., 2019. Object-based change detection using multiple classifiers and multi-scale uncertainty analysis. Remote Sensing 11 (3), 359. https://doi.org/10.3390/rs11030359.

Tao, Q., Wu, G.-W., Wang, F.-Y., Wang, J., 2005. Posterior probability support vector machines for unbalanced data. IEEE Trans. Neural Networks 16 (6), 1561–1573.

van Duynhoven, A., Dragićević, S., 2019. Analyzing the effects of temporal resolution and classification confidence for modeling land cover change with long short-term memory networks. Remote Sensing 11 (23), 2784. https://doi.org/10.3390/rs11232784.

Verbesselt, J., Hyndman, R., Newnham, G., Culvenor, D., 2010. Detecting trend and seasonal changes in satellite image time series. Remote Sens. Environ. 114 (1), 106–115.

Volpi, M., Tuia, D., Bovolo, F., Kanevski, M., Bruzzone, L., 2013. Supervised change detection in VHR images using contextual information and support vector machines. Int. J. Appl. Earth Obs. Geoinf. 20, 77–85.

Wang, X., Du, P., Chen, D., Lin, C., Zheng, H., Guo, S., 2020a. Characterizing urbanization-induced land surface phenology change from time-series remotely sensed images at fine spatio-temporal scale: A case study in Nanjing, China (2001–2018). J. Cleaner Prod. 274, 122487. https://doi.org/10.1016/j.jclepro.2020.122487.

Wang, X., Du, P., Chen, D., Liu, S., Zhang, W., Li, E., 2020b. Change detection based on low-level to high-level features integration with limited samples. IEEE J. Sel. Top. Appl. Earth Obs. Remote Sens. 13, 6260–6276.

Wang, X., Fan, X., Xu, Q., Du, P., 2022. Change detection-based co-seismic landslide mapping through extended morphological profiles and ensemble strategy. ISPRS J. Photogramm. Remote Sens. 187, 225–239.

Woodcock, C.E., Loveland, T.R., Herold, M., Bauer, M.E., 2020. Transitioning from change detection to monitoring with remote sensing: A paradigm shift. Remote Sens. Environ. 238, 111558. https://doi.org/10.1016/j.rse.2019.111558.

Wu, C., Du, B.o., Cui, X., Zhang, L., 2017. A post-classification change detection method based on iterative slow feature analysis and Bayesian soft fusion. Remote Sens. Environ. 199, 241–255.

Wulder, M.A., Loveland, T.R., Roy, D.P., Crawford, C.J., Masek, J.G., Woodcock, C.E., Allen, R.G., Anderson, M.C., Belward, A.S., Cohen, W.B., Dwyer, J., Erb, A., Gao, F., Griffiths, P., Helder, D., Hermosilla, T., Hipple, J.D., Hostert, P., Hughes, M.J., Huntington, J., Johnson, D.M., Kennedy, R., Kilic, A., Li, Z., Lymburner, L., McCorkel, J., Pahlevan, N., Scambos, T.A., Schaaf, C., Schott, J.R., Sheng, Y., Storey, J., Vermote, E., Vogelmann, J., White, J.C., Wynne, R.H., Zhu, Z., 2019. Current status of Landsat program, science, and applications. Remote Sens. Environ. 225, 127–147.

Xian, G., Homer, C., 2010. Updating the 2001 National Land Cover Database impervious surface products to 2006 using Landsat imagery change detection methods. Remote Sens. Environ. 114 (8), 1676–1686.

Zalles, V., Hansen, M.C., Potapov, P.V., Parker, D., Stehman, S.V., Pickens, A.H., Parente, L.L., Ferreira, L.G., Song, X.-P., Hernandez-Serna, A., Kommareddy, I., 2021. Rapid expansion of human impact on natural land in South America since 1985. Science. Advances 7 (14). https://doi.org/10.1126/sciadv.abg1620.

ZhiYong, L.v., Wang, FengJun, Xie, LinFu, Sun, WeiWei, Falco, N., Benediktsson, J.A., You, ZhenZhen, 2021. Diagnostic analysis on change vector analysis methods for LCCD using remote sensing images. IEEE J. Sel. Top. Appl. Earth Obs. Remote Sens. 14, 10199–10212.

Zhu, Z., 2017. Change detection using landsat time series: A review of frequencies, preprocessing, algorithms, and applications. ISPRS J. Photogramm. Remote Sens. 130, 370–384.

Zhu, Z., Woodcock, C.E., 2014. Continuous change detection and classification of land cover using all available Landsat data. Remote Sens. Environ. 144, 152–171.